Strategies for novel transparent conducting sol gel oxide coatings

A. Kurz, K. Brakecha, J. Puetz, M.A. Aegerter *

Leibniz-Institut für Neue Materialien, Department of Coating Technology, Im Stadtwald, 66123 Saarbrücken, Germany

Abstract

Transparent conducting coatings of doped SnO_2 and Zn_2SnO_4 have been deposited by the sol gel technique on borosilicate and alumosilicate glass substrates, respectively. As films of SnO_2:Sb (ATO) show some intrinsic drawbacks, which are discussed in this report, alternative dopants for SnO_2 such as Ta, Nb and W, were examined concerning the electrical and optical properties of the deposited coatings. In this way, coatings with resistivities on the order of 3×10^{-2} Ω cm characterized by much higher charge carrier mobilities than for SnO_2:Sb and a transmission of >85% were realized. In the search for ternary compounds ($A_xB_yO_z$), coatings in the system ZnO SnO_2 were examined, focusing on the fabrication of meta zinc stannate (Zn_2SnO_4). Coatings made from tin alkoxides yielded monophasic materials with high crystallinity and good morphological properties. By post annealing, a resistivity of 0.4 Ω cm with charge carrier mobilities of up to 7 cm^2/Vs were obtained. Therefore, the development of the coating solution is as crucial as the elaboration of the heat treatment procedure of as deposited films in order to obtain pure Zn_2SnO_4 phase coatings without any impurity phases.

Keywords: Transparent conducting oxide; Tin oxide; Zn_2SnO_4; Sol gel

1. Introduction

Rapid developments in today's electronic devices including flat panel displays and touch panels are asking for highly sophisticated components, with an ever-increasing performance. The development of transparent conducting coatings as electrodes with customized characteristics like high electron work function, high electron mobility and high transparency, hence, is becoming more and more relevant [1]. To meet these forthcoming requirements, however, novel materials or improved coating techniques are in need. One of these approaches is focusing on a combination of several coating methods, as for example, magnetron sputtering and sol–gel dip coating, to benefit from the advantages of both techniques [2].

In search of new sol–gel processed TCO materials, there are essentially two ways to cope with the task of finding new TCOs that meet the above mentioned requirements:

- taking advantage of known TCO systems, as e.g., antimony doped tin oxide (ATO, $SnOB_2$:Sb) and modifying the composition or doping,
- looking for more sophisticated ternary or quaternary phases among 'common' TCO host materials. As considerable effort has been directed to 'common' TCO materials, whose properties are restricted to the intrinsic characteristics of their underlying binary oxides, new compounds with tailored functionalities could prove important.

Antimony doped tin oxide, as the most commonly used sol–gel TCO material, suffers from some short-comings of the Sb dopant and its electronic and optical properties have almost reached the physical limits of the material, with little scope for further improvements. As Sb has two stable high-valent oxidation states, i.e. Sb^{III} and Sb^V, there is a tendency to form an equilibrium between these two valences during film formation, with the equilibrium position being influenced by the oxidation state of the starting material [3–5].

Though Sb^V generally is found to be the most stable oxidation state in a SnO_2 host matrix [4], porous ATO materials, including nanoparticles and sol–gel films, suffer from the grainy structure and the resulting high surface area, which involves an enrichment of Sb^{III} and Sb^V species at the particle surfaces [5]. As only Sb^V is effectively contributing to an increase of the charge carrier density and hence of the conductivity, whereas Sb^{III} is supposed to act as an electron trap thus showing an opposite effect especially if situated at the surface of the grains, there is a significant loss of doping efficiency in the films [5]. A loss of antimony due to a volatilization during film formation [6], however, can be largely excluded, as the total amount of antimony in the films is in accordance with the experimental values [7]. The segregation of dopant at the surface of the doped SnO_2 grains furthermore results in a restriction of crystal growth (and hence a further increase of the surface area) during sintering compared to pure SnO_2 and in a significant increase of the grain boundary scattering due to an electron depletion layer [3,8]. In consequence, the charge carrier mobility and the observed conductivity of such materials are comparatively low. The coexistence of Sb^{III} and Sb^V at last can also be regarded as the reason for the bluish coloration and the reduced transmission at high film thickness [9], which otherwise is used in greyish-blue tin-antimony pigments for glazes [10]. This intense absorption in the red and the near infrared frequently has been attributed to an electronic transfer between the different oxidation states [9,11,12], but is most probably due to a free charge carrier absorption in the semiconducting material [3]. The antimony thus is not directly involved in the NIR absorption, but rather through its influence on the particle morphology by limiting the grain size and increasing the grain boundary scattering which then lead to a change in the plasma absorption band. Though this was shown specifically for ATO nanoparticle coatings [3], a similar behaviour is to be expected for the sol–gel ATO coatings with their loose and grainy structure of small crystallites.

As part of the Sb is found as a separate oxide phase at the surface of the SnO_2 rather than incorporated in the matrix, also the lower chemical and mechanical stability of the Sb oxide phases and especially the general toxicity of Sb come into play and often limit the application of ATO.

Doping alternatives for Sb in $SnO_2:Sb$ ideally should have only one single stable oxidation state of V or VI and an ionic radius comparable with that of Sn^{IV} in the host material to avoid lattice distortion and related scattering effects. Therefore, transition metals of groups Vb and VIb should be promising candidates for this task which will be discussed in Section 3.1.

A second approach to new TCO materials, as mentioned above, is the investigation of 2- and 3-dimensional phase spaces made up of known TCO compounds, but also involving other metal oxides. As the preparation of multinary, single-phase compounds from a multi-precursor system is a challenging task, only little work has obviously
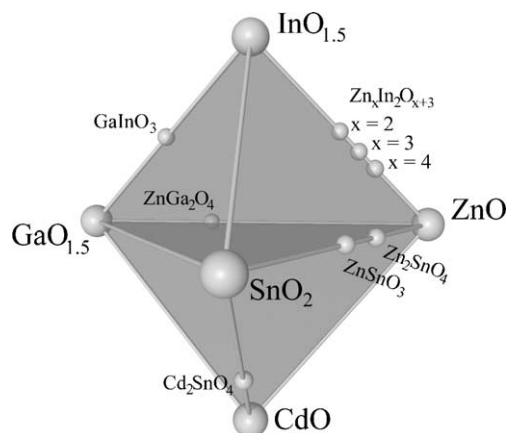

Fig. 1. Schematic multidimensional phase diagram of 'common' TCO host materials.

been done so far in the field of sol–gel TCO synthesis of such materials. As a consequence, there is a heavy lack of experience which otherwise is essential to tailor state-of-the-art materials with special properties.

The schematic phase diagram in Fig. 1 gives an example of a promising multidimensional phase-space where several ternary compounds with interesting properties are known to exist, including Cd_2SnO_4, Zn_2SnO_4, $ZnSnO_3$ and $ZnGa_2O_4$.

As early as the 1970s, Nozik [13] and Haacke et al. [14] reported on the preparation of sputtered Cd_2SnO_4 (CTO) coatings for use in TCO applications. The material shows extraordinary high electron mobilities (up to 80 cm^2/Vs [15]) combined with a high transmission in the visible which makes it particularly suited as front electrodes in solar cells [16]. As an alternative for this highly toxic Cd compound, however, research efforts have also been directed to sputtered Zn_2SnO_4 (meta zinc stannate) [15,17–19], which exhibits a similar crystal structure (inverse spinel [20]), but with inferior electrical properties compared to CTO. Another promising phase in the $ZnO–SnO_2$ system is $ZnSnO_3$ (ortho zinc stannate), which is known for its high electron work function (up to 5.4 eV) [21]. However, this phase is not thermally stable and decomposes into Zn_2SnO_4 and SnO_2 at higher temperatures (~300–400 °C). Other ternary compounds of interest are, for example, $Zn_2In_2O_5$, $MgIn_2O_4$, $In_4Sn_3O_{12}$ and $GaSbO_4$ [22]. TCO materials based on 'non-TCO' compounds include e.g. In_6WO_{12} [23] and p-type $CuAlO_2$ [24].

In this paper, mainly initial experiments are presented, focusing on the search of appropriate precursor systems leading to monophasic compounds in the system $ZnO–SnO_2$.

2. Experimental

In the case of doped tin oxide coatings, the coating solutions were prepared by dissolving $SnCl_2(OAc)_2$ (prepared according to Ref. [25]) and the corresponding chlorides or oxychlorides of the doping elements in ethanol adding 5 vol.% of 2-isopropoxyethanol (IPE) as a
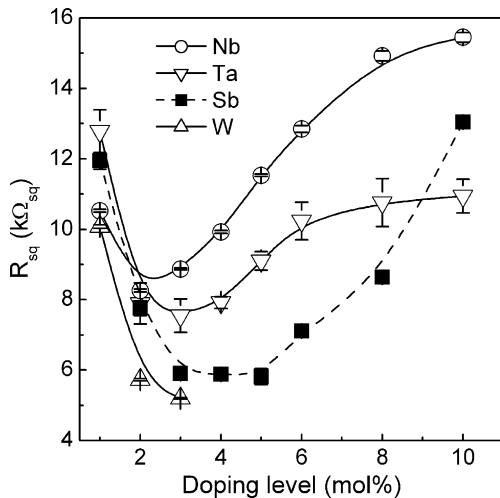
Fig. 2. Sheet resistance as a function of doping level for SnO_2 films with different dopants (thicknesses approx. 55 nm).

stabilizing agent. The dopant concentration ranged from 1 to 10 mol% while the total tin concentration was fixed at 0.25 mol/l. Coating solutions for the ternary TCO compounds were prepared by dissolving the appropriate amounts of metal chlorides or alkoxides in ethanol. All solutions had a zinc to tin molar ratio [Zn]/([Zn]+[Sn]) ranging from 0.3 to 0.9 and a total metal concentration of 0.4 mol/l. In both cases, the solutions were heated under reflux for 1 h and filtered (0.2 μm PTFE) before deposition.

The tin oxide coatings were deposited by dip-coating (4 mm/min) on alkaline-free alumosilicate glass substrates (AF45 Schott-DESAG) with a size of 10×6 cm^2 and heat-treated for 15 min at 550 °C in air, while the ternary oxide coatings were spin-deposited (1000 rpm) on borosilicate glass substrates (Borofloat 33 Schott/Jenaerglas) with a size of 5×5 cm^2 followed by a heat treatment at $550-600$ °C for $1-24$ h using a heating rate of 5 K/min. In the latter case, a further annealing in reducing atmosphere (80% N$_2$/ 20% H$_2$) was performed during 1 h at 300 °C in a gas flow of 100 l/h.

X-ray diffraction (XRD) patterns were obtained on a Siemens D500 diffractometer equipped with a thin film sample holder in the 2θ range between 10° and 70° at grazing incidence ($\theta = 0.5°$) using CuK$_\alpha$ radiation. Crystallite sizes could be extracted from Williamson–Hall plots using integral widths of suitable diffraction peaks [26]. Thickness measurements were performed with a surface profiler (TENCOR P-10) after etching a sharp edge with concentrated HCl and zinc powder. A scanning electron microscope equipped with an EDX unit (JSM 6400 F, JEOL) was used to obtain images of the coating surfaces (excitation energy 10 keV) and to determine the elemental composition of the coatings from the EDX spectra (excitation energy 15 keV). Haze and transmittance values were measured with a haze-meter (BYK Gardner Hazegard plus) in reference to haze and clarity standards. Transmission and reflection spectra were collected on a

spectrophotometer (Varian CARY 5E) in the range from 200 to 3000 nm against air as a reference. Electrical properties (resistivity, Hall mobility, charge carrier density) were measured by means of the Van der Pauw and Hall method (MMR Technologies) using a magnetic field of 1.3 T. The sheet resistance $R_\square$ of the films was measured by the four-point probe technique (gold tips, 3 mm spacing). The surface roughness was evaluated by AFM (Topomatrix Explorer TMX2000) in contact mode equipped with an ultra-sharp Si$_3$N$_4$ cantilever (ND-MDT) over an area of 500×500 nm^2.

3. Results

3.1. Doped tin oxide

To overcome typical drawbacks of SnO_2:Sb thin films, dopants from the transition metal groups Vb (V, Nb, Ta) and VIb (Mo, W) were investigated. The variation of resistivity with doping concentration (mol%) as plotted in Fig. 2 for the investigated dopants, shows three potential doping elements as alternatives for an antimony doping. The minimum sheet resistance of Ta- and Nb-doped thin films (7.5 k$\Omega_\square$ and 8.5 k$\Omega_\square$, respectively) is achieved for 2 mol%, whereas the optimum doping level for SnO_2:W films lies in the concentration range between 2 and 3 mol% and gives the lowest sheet resistance of 5.2 k$\Omega_\square$ (2.9×10^{-2} Ω cm, 55 nm). The resistivity of SnO_2:Sb reaches similar values of 6 k$\Omega_\square$ but shows a broader minimum at higher doping levels (3 to 5 mol%) suggesting a lower doping efficiency of antimony. A closer examination of the electrical parameters of the coatings (Table 1), however, reveals fundamental differences in the doping mechanisms of Sb and the transition metals. In the case of Sb, the minimum resistivity is mainly sustained by a high charge carrier density with a very low mobility of only 1.5 to 2 cm^2/Vs, while the transition metal doping results in a significantly higher mobility up to 7 cm^2/Vs at a comparably low charge carrier density. As already discussed before, this restriction of the charge carrier mobility and the comparably high doping level for ATO finally are both attributed to the coexistence of Sb^{III} and Sb^V [3,5], i.e. the formation of an antimony-rich, electron-depleted layer at the surface of the grains or

Table 1
Typical electrical properties of doped SnO_2 thin films (doping level at the minimum of resistivity)

Material	Doping level (mol%)	Thickness (nm)	Resistivity (10^{-2} Ωcm)	Mobility (cm^2/Vs)	Carrier density (10^{19} cm^{-3})
SnO_2		50	20	~30	0.1
SnO_2:Sb	5	51	3.1	1.5 2	10
SnO_2:Nb	2	50	4.0	7	2.2
SnO_2:Ta	2	52	3.9	5	3.2
SnO_2:W	3	55	2.9	6	3.6

Table 2
Effective ionic radii (octahedral coordination) of Sn (SnO_2) and of different doping materials [27]

Metal	Oxidation state	Ionic radius (pm)
Sn	IV	69
Sb	III	76
	V	60
Nb	IV	68
	V	64
Ta	IV	68
	V	64
W	IV	66
	V	62
	IV	60
V	IV	58
	V	54
Mo	IV	65
	V	61
	VI	59

crystallites leads not only to an increased grain boundary scattering but also to a diminution of the charge carrier density inside the grain.

Contrary to the original idea to avoid these problems by using more stable, high-valent dopants, however, a doping with Ta, Nb or W did not result in a higher charge carrier density, but rather in a significantly increased electron mobility. Even if this higher mobility to a certain extent is a consequence of the lower charge carrier density, also a change in the surface layer has to be considered as a possible cause. As these dopants are characterized by stable oxidation states of 5+ (Ta, Nb) or 5+ to 6+ (W), both the loss of dopant atoms by formation of lower-valent species and the effect of electron traps at the surface should be principally eliminated.

Besides the oxidation state, however, the ionic radius of the doping element is an essential requirement for a suitable dopant. It should be on the order of the ionic radius of Sn^{IV} (69 pm) to avoid lattice distortion of the SnO_2 host lattice, when a tin atom is replaced with a dopant atom. Since Ta^V, Nb^V, and W^{VI} have similar ionic radii as Sn^{IV} (Table 2 [27]), they can easily substitute Sn in the SnO_2 host lattice.

In accordance with these considerations, vanadium doped films did not show any electrical conductivity, as the ionic radius of vanadium in all oxidation states is significantly smaller compared to its homologues Nb and Ta (Table 2). Moreover, the preferred oxidation state of vanadium in the tin oxide host lattice seems to be the 4+ rather than the 5+ state [28] so that an efficient doping is not possible. In the case of Mo, however, no conductivity could be observed though the ionic radius is very similar to that of W, and the reason for the missing conductivity thus is rather expected in differences in the electronic structure of the ions.

At higher doping levels, the electrical resistivity increases again for all investigated dopants, as the excess dopant atoms start to act as scattering centres thus lowering the mobility of the carriers. Additionally, the tendency for phase separation and segregation of dopant atoms at the surface of the SnO_2 grains is likely to increase the grain boundary scattering and thus to further reduce the charge carrier mobility while at the same time the charge carrier density is reduced.

Besides the influence on the electrical properties, the novel dopants also lead to an improvement in the optical properties of the films, as shown in Fig. 3. SnO_2:Sb films show a strong absorption in the upper part of the visible and the near infrared range, related to a free charge carrier absorption. In contrast, SnO_2 films with Nb-, Ta-, or W-doping only exhibit a slight decrease in transmission for wavelengths up to 2000 nm, and the SnO_2:Nb films even have a transmittance that is comparable to that of undoped SnO_2 films. These superior optical properties of Nb-, Ta- and W-doped SnO_2 films compared to ATO films can be explained both by the lower charge carrier density and the higher charge carrier mobility leading to a shift of the plasma absorption band towards the IR and a steeper rise, respectively. As a result, the absorption does not occur in the visible and the obtained films are almost colorless with only a slight yellowish shade, due to the absorption near the band edge.

Another advantage of the novel doping elements is the lower toxicity and the higher chemical stability as compared to Sb-doped films. Both factors expand the spectrum of possible applications of doped SnO_2 coatings.

3.2. Ternary TCO compounds

The search for sol–gel ternary compounds in the ZnO–SnO_2 system was initially concentrating on the investigation of the coating solution. Fig. 4 shows the influence of the composition of the coating solution on the resulting
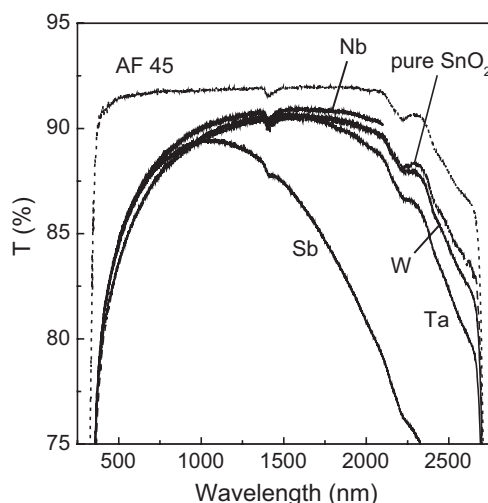

Fig. 3. Transmission spectra of SnO_2 sol gel films without doping and with Nb-, Ta-, W- and Sb-doping (double sided coating on AF45 glass).
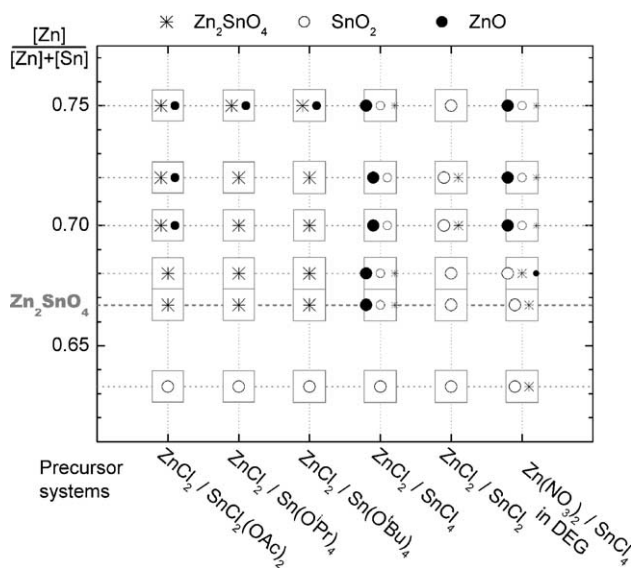
Fig. 4. Influence of precursors and zinc to tin ratio (0.63–0.75 range) in coating solutions on thin film phase formation as observed by XRD measurements (solvent: ethanol, except column 6: diethylene glycol (DEG); heat-treatment 550 °C for 24 h at 5 K/min). Each square represents a coating. The crystalline phases observed for each film are indicated by the symbols $*$ (Zn_2SnO_4), $\bigcirc$ (SnO_2) and $\bullet$ (ZnO), the amount of phase decreasing from left to right in each square. The dashed horizontal line represents the theoretical ratio of zinc to the total metal content in Zn_2SnO_4 (2/3).

Fig. 6. Characteristic XRD diagrams of coatings in the system ZnO–SnO_2, including reference data from the ICDD PDF2 database where appropriate.

crystalline phases, focusing on the composition ratios for the formation of Zn_2SnO_4. As it can be seen, most coating solutions yielded multiphase coatings with variable composition, and monophasic Zn_2SnO_4 could only be obtained by the use of tin precursors with a strong tendency to polymerize upon condensation (i.e. $SnCl_2(OAc)_2$, $Sn(O^iPr)_4$ and $Sn(O^tBu)_4$).

Besides the phase composition, also the homogeneity and morphology of the coatings is of importance for their use as TCO films. For comparison, Fig. 5(a) and (b) shows the surface morphology of coatings made from coating solutions containing $SnCl_2(OAc)_2$ and $Sn(O^tBu)_4$, respectively.

As can be seen in Fig. 5(a), large agglomerates with diameters of approx. 500 nm are formed in the case of the $SnCl_2(OAc)_2$ precursor. These agglomerates are already visible in the as-deposited coatings and are most probably due to wetting problems of the $ZnCl_2$ component during the drying of the film. As these coatings were hazy in appearance (haze ~15%), the influence of different solution additives (e.g. glycols and glycol ethers) to modify the solution properties (wetting, levelling, etc.) and to enhance the coating quality, was investigated. It was found that additives strongly influence the surface roughness and homogeneity, but at the same time also determine the crystallinity of the deposited coatings, i.e. in cases where coatings with low haze values below 1% could be obtained, no crystalline phase could be identified. In contrast, a similar coating morphology as in Fig. 5(a) is not observed in tin alkoxide based coatings (Fig. 5(b)) which show a very smooth and homogeneous surface.
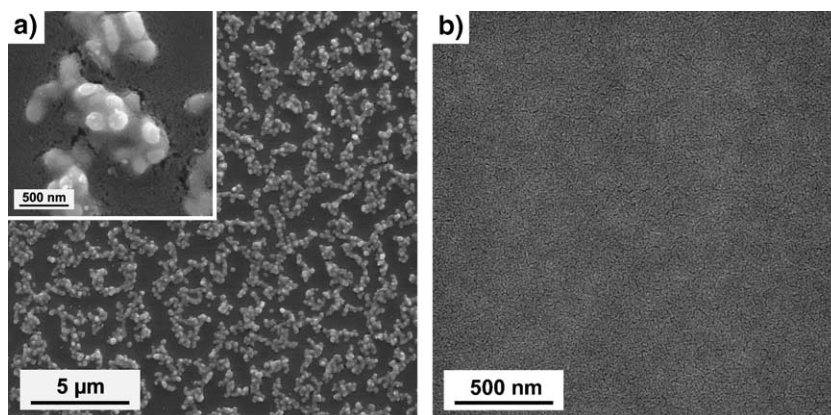

Fig. 5. SEM images of sintered coatings (550 °C/24 h, heated at 5 K/min) made from ethanolic solutions of $ZnCl_2$ with (a) $SnCl_2(OAc)_2$ and (b) $Sn(O^tBu)_4$. Total metal content: 0.4 mol/l, [Zn]/([Zn]+[Sn]) 0.7.
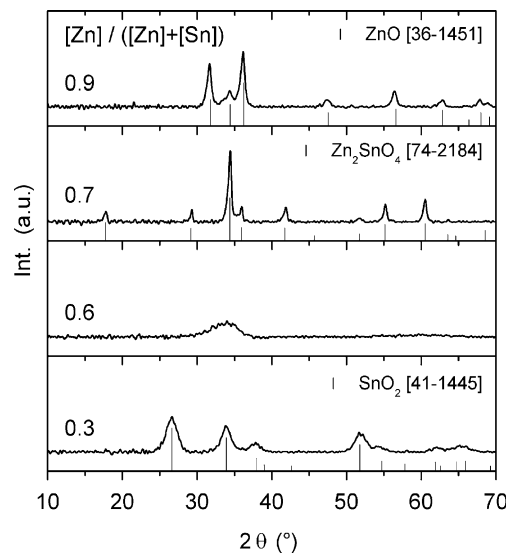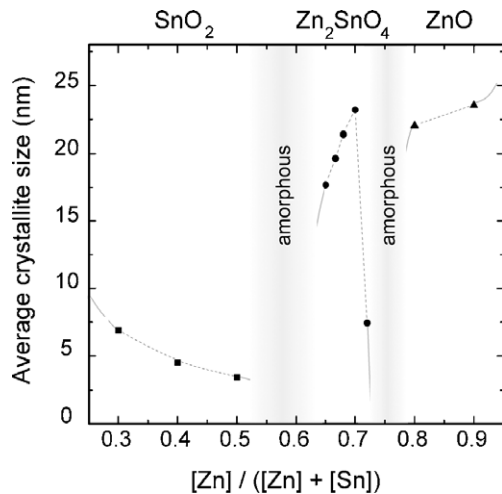
Fig. 7. Influence of the $[Zn]/([Zn]+[Sn])$ ratio on phase formation and crystallite sizes in the coatings. Coating solutions contained $ZnCl_2/Sn(O^tBu)_4$ in ethanol with a total metal content of 0.4 mol/l resulting in coating thicknesses of (73 ± 4) nm. As-deposited coatings were heat-treated at 600 °C for 2 h (2 K/min).

Coatings made from solutions containing $ZnCl_2$ and $Sn(O^tBu)_4$ in various ratios show Zn_2SnO_4 crystallites with a size of up to 23 nm after sintering at 600 °C for 2 h (2 K/min). Fig. 6 shows XRD diagrams of observed phases in the $ZnO-SnO_2$ system and as can be seen from Fig. 7, monophasic Zn_2SnO_4 with varying crystallite sizes can be obtained from solutions with a $[Zn]/([Zn]+[Sn])$ ratio between 0.65 and 0.72.

As all Zn_2SnO_4 coatings showed resistivities >15 kΩ cm right after the sintering process in air, a second heat treatment was performed in reducing atmosphere ($N_2:H_2=80:20$) at 300 °C for 1 h at a gas flow rate of 100 l/h to promote the formation of oxygen vacancies. Following this procedure, a resistivity of 0.4 Ω cm could be achieved for crystalline coatings with a thickness of 35 nm at a $[Zn]/([Zn]+[Sn])$ ratio of 0.7 after a pre-treatment in air at 600 °C for 2 h. Similar resistivities were observed for thicker, amorphous films of 95 nm (pre-treatment for 1 h), but with higher mobilities of 7.7 cm^2/Vs compared to 2.44 cm^2/Vs for crystalline coatings. Accordingly, the charge carrier density was found to be higher for crystalline films (6.4×10^{18} cm^{-3} compared to 1.6×10^{18} cm^{-3}). All coatings exhibited haze values $<1\%$, an average transmission in the visible range $>85\%$ and an average roughness $R_a < 1$ nm for thicknesses in the range of 35 to 200 nm.

4. Conclusions

In search of novel sol–gel TCO materials, two different strategies were followed. To overcome the intrinsic drawbacks of the antimony doping in $SnO_2:Sb$ films, transition metals of groups Vb and VIb were found to be highly effective alternative dopants. Best results were obtained with Nb^V-, Ta^V- and W^{VI}-doping of SnO_2 with a resistivity of $3-4 \times 10^{-2}$ Ω cm, comparable to that of $SnO_2:Sb$ but at much lower doping levels. Corresponding coatings show a significantly higher transmission ($>85\%$) in the visible with no coloration and moreover exhibit a lower toxicity and higher chemical stability compared to $SnO_2:Sb$ coatings.

As a new ternary sol–gel TCO material, monophasic Zn_2SnO_4 was successfully deposited in optical quality on glass substrates. It was shown that it is most crucial to adjust the composition of the coating solution as well as the process parameters in order to obtain polycrystalline meta zinc stannate (Zn_2SnO_4). As the electrical properties of the coatings strongly depend on the crystallographic and morphological properties, the resistivity of a 35 nm-thick Zn_2SnO_4 coating thus is limited to typically 0.4 Ω cm. Reduced Hall mobilities in polycrystalline coatings are probably due to an increased electron scattering at grain boundaries.

References

[1] A.J. Freeman, K.R. Poeppelmeier, T.O. Mason, R.P.H. Chang, T.J. Marks, MRS Bull. 25 (2000) 45.
[2] G. Guzman, B. Dahmani, J. Puetz, M.A. Aegerter, Thin Solid Films (this issue), doi:10.1016/j.tsf.2005.07.297.
[3] T. Nütz, M. Haase, J. Phys. Chem., B 104 (2000) 8430.
[4] J. Rockenberger, U. zum Felde, M. Tischer, L. Tröger, M. Haase, H. Weller, J. Chem. Phys. 112 (2000) 4296.
[5] C. McGinley, H. Borchert, M. Pflughoefft, S. Al Moussalami, A.R.B. de Castro, M. Haase, H. Weller, T. Möller, Phys. Rev., B 64 (2001) 245312.
[6] G. Gasparro, J. Pütz, D. Ganz, M.A. Aegerter, Sol. Energy Mater. Sol. Cells 54 (1998) 287.
[7] K. Brakecha, Diploma thesis, Leibniz-Institut fuer Neue Materialien, 2005.
[8] G. Boschloo, D. Fitzmaurice, J. Phys. Chem., B 103 (1999) 3093.
[9] M. Kojima, H. Kato, G. Mitsuru, Philos. Mag., B 68 (1993) 215.
[10] C. Fontanesi, C. Leonelli, T. Manfredini, C. Siligardi, G.C. Pellacani, J. Eur. Ceram. Soc. 18 (1998) 1593.
[11] E. Elangovan, K. Ramamurthi, Cryst. Res. Technol. 387 (2003) 779.
[12] C. Terrier, J.P. Chatelon, R. Berjoan, J.A. Roger, Thin Solid Films 263 (1995) 37.
[13] A.J. Nozik, Phys. Rev., B 6 (1972) 453.
[14] G. Haacke, W.E. Mealmaker, L.A. Siegel, Thin Solid Films 55 (1978) 67.
[15] T.J. Coutts, D.L. Young, X. Li, W.P. Mulligan, X. Wu, J. Vac. Sci. Technol., A, Vac. Surf. Films 18 (2000) 2646.
[16] X. Wu, P. Sheldon, T.J. Coutts, D.H. Rose, H. Moutinho, Proc. of the 26th IEEE Photovoltaic Specialists ConferenceAnaheim, California, September 29-October 3, 1997, p. 347.
[17] H. Enoki, T. Nakayama, J. Echigoya, Phys. Status Solidi, A Appl. Res. 129 (1992) 181.
[18] D.L. Young, H. Moutinho, Y. Yan, T.J. Coutts, J. Appl. Phys. 92 (2002) 310.
[19] J. Perkins, J. del Cueto, J. Alleman, C. Warmsingh, B. Keyes, L. Gedvilas, P. Parilla, B. To, D. Readey, D.S. Ginley, in: I. Takeuchi, J.M. Newsam, L.T. Wille, H. Koinuma, E.J. Amis (Eds.), Combinatorial and Artificial Intelligence Methods in Materials Science, Boston, Massachusetts, November 26 30, 2001, Mat. Res. Soc. Symp. Proc., vol. 700, 2002 (S1.9.1.).
[20] S.H. Wei, S.B. Zhang, Phys. Rev., B 6304 (2001) 5112.

218

[21] T. Minami, T. Miyata, T. Yamamoto, Surf. Coat. Technol. 109 (1998) 583.
[22] T. Minami, MRS Bull. 25 (2000) 38.
[23] W.S. Dabney, N.E. Antolino, B.S. Luisi, A.P. Richard, D.D. Edwards, Thin Solid Films 411 (2002) 192.
[24] H. Kawazoe, H. Yanagi, K. Ueda, H. Hosono, MRS Bull. 25 (2000) 28.
[25] E. Ruf, German Patent No. DE4005135A1, 17 Feb. 1990.
[26] G.K. Williamson, W.H. Hall, Acta Metall. 1 (1953) 22.
[27] R.D. Shannon, Acta Crystallogr., A 32 (1976) 751.
[28] S. Bordoni, F. Castellani, F. Cavani, F. Trifiro, M. Gazzano, J. Chem. Soc., Faraday Trans. 90 (1994) 2981.